

Mixing of dielectronic and multiply excited states in electron–ion recombination: a study of Au²⁴⁺

G F Gribakin and S Sahoo

Department of Applied Mathematics and Theoretical Physics, Queen's University of Belfast, Belfast BT7 1NN, UK

E-mail: g.gribakin@am.qub.ac.uk and s.sahoo@am.qub.ac.uk

Received 27 May 2003

Published 18 July 2003

Online at stacks.iop.org/JPhysB/36/3349

Abstract

It has been suggested (Gribakin *et al* 1999 *Aust. J. Phys.* **52** 443–57, Flambaum *et al* 2002 *Phys. Rev. A* **66** 012713) that strongly enhanced low-energy electron recombination observed in Au²⁵⁺ (Hoffknecht *et al* 1998 *J. Phys. B: At. Mol. Opt. Phys.* **31** 2415–28) is mediated by complex multiply excited states, while simple dielectronic excitations play the role of doorway states for the electron capture process. We present the results of an extensive study of configuration mixing between doubly excited (doorway) states and multiply excited states which account for the large electron recombination rate on Au²⁵⁺. A detailed analysis of spectral statistics and statistics of eigenstate components shows that the dielectronic doorway states are virtually 'dissolved' in complicated chaotic multiply excited eigenstates. This work provides a justification for the use of statistical theory to calculate the recombination rates of Au²⁵⁺ and similar complex multiply charged ions. We also investigate approaches which allow one to study complex chaotic many-body eigenstates and criteria of strong configuration mixing, without diagonalizing large Hamiltonian matrices.

1. Introduction

The aim of this paper is to study the details of configuration mixing between doubly excited and more complicated many-electron states populated in the process of recombination of a low-energy electron with a heavy multiply charged ion, Au²⁵⁺.

Recombination of electrons with multiply charged ions is of fundamental importance in different areas of modern physics. Cross sections and rate coefficients for the process are particularly needed for the understanding of astrophysical and fusion plasmas, and also provide useful information for the application in ion storage rings. The basic recombination process provides a unique testing ground for atomic structure calculations and atomic collision theory. It is usually considered in terms of two main mechanisms: radiative recombination (RR) and

dielectronic recombination (DR). RR is the direct capture of a free electron by an ion, where the excess energy is carried away by a photon. The electron can also be captured resonantly, when the excess energy is used to excite an electron within the target ion. This capture is only possible if the kinetic energy of the incident electron is close to the difference between the total energy of the excited state of the compound ion and that of the initial state of the target ion. In this process the compound ion is formed in a multiply (usually doubly) excited state. Its subsequent decay by emission of a photon is known as DR.

Our present understanding of the role and details of DR is the result of a long, fruitful and competitive development of theory and experiment. Its achievements are well documented in Graham *et al* (1992) and a more recent review paper by Hahn (1997). However, in spite of more than half a century of study 'there are still serious difficulties with the low-energy recombination process [...] which are not yet fully understood' (Hahn 1997). We address one of them in this paper.

The major difference between RR and DR is that the latter is a resonant process. Its contribution often reveals a rich structure, usually in the form of narrow peaks, over the smooth RR background. This energy dependence together with an overall enhancement of the (energy-averaged) recombination rate are the hallmarks of DR. This picture has become increasingly clear and detailed through the results obtained in merged-beams experiments with ion accelerators and storage rings (see, e.g., Müller 1999). Narrow energy spreads of electron beams, down to 1 meV (Lindroth *et al* 2001), allow one to analyse the resonances populated in the process of electron capture by the target ion and obtain unique information about complex highly correlated doubly (or multiply) excited states of the compound ion with energies above the ionization threshold. For example, the DR spectrum of C^{3+} revealed strong relativistic effects (Mannervik *et al* 1998), and that of Pb^{53+} provided a test of quantum electrodynamics in a many-electron system (Lindroth *et al* 2001), while a study of Sc^{3+} was geared towards observing interference effects between direct and resonant recombination, or between adjacent DR resonances (Schippers *et al* 2002).

There are two other interesting phenomena in low-energy electron recombination. The first one is an enhancement of the recombination rate at very low electron energies ($\varepsilon \lesssim 1$ meV). The 'excess' rate at $\varepsilon = 0$ increases with the charge of the ion ($\propto Z_i^{2.8}$ for light ions, Gao *et al* (1997)), scales as $T_{\perp}^{-1/2}$ and $T_{\parallel}^{-1/2}$ with the transversal and longitudinal temperatures of the electron beam, increases strongly with the magnetic field, but is insensitive to the electron density (Hoffknecht *et al* 1998, Gwinner *et al* 2000). Since this effect is observed for bare as well as many-electron ions (Gao *et al* 1997, Uwira *et al* 1997, Hoffknecht *et al* 2000), its origins are not related to electron correlations or the structure of the target ion. A recent paper by Heerlein *et al* (2002) suggests that this enhancement comes from high-lying Rydberg states populated due to an external field effect on the merging ion and electron beams.

The second phenomenon is a huge *uniform* enhancement of the recombination rate over the RR rate observed for Au^{25+} over a wide range of energies (Hoffknecht *et al* 1998). The energy dependence of the rate at $\varepsilon \sim 1$ eV is similar to that of RR, but the magnitude is about 200 times greater. What is equally puzzling is that the data taken with an energy resolution of about 0.1 eV do not show any DR-type resonant features or, for that matter, any structure at all, except two broad maxima around 30 and 80 eV.

To resolve this puzzle, Gribakin *et al* (1999) investigated the spectrum of multiply excited states of Au^{24+} near the ionization threshold. These states can play a role in the process of electron capture by Au^{25+} and, after emission of a photon, lead to recombination. Gribakin *et al* (1999) showed that, due to a 'gapless' electron orbital spectrum and open-shell structure of the system (the ground state of Au^{24+} belongs to the $4f^9$ configuration), the excitation spectrum of this ion is extremely dense. They found that the mean spacing D between multiply excited

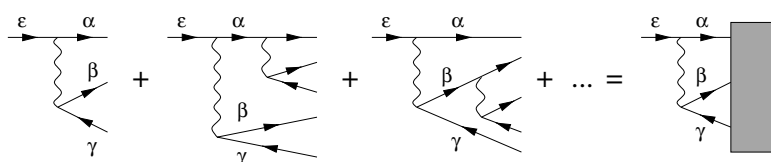


Figure 1. Schematic diagram of electron capture into a complex multiconfigurational eigenstate (shaded block) through a dielectronic doorway configuration $\gamma^{-1}\alpha\beta$. Wavy lines show the electron Coulomb interaction and the sum of diagrams on the left-hand side corresponds to a non-perturbative (CI) calculation of the capture amplitude.

states with a given angular momentum and parity, J^π , near the ionization threshold is very small, $D \sim 1$ meV, and concluded that the system was characterized by extremely strong, in some sense complete and ‘chaotic’, configuration mixing. This mixing is characterized by an energy interval $\Gamma \sim 0.5$ au, called the spreading width. As a result, the eigenstates should typically contain $\Gamma/D \gtrsim 10^4$ basis state components and the process of electron capture is mediated by complex multiply excited states rather than simple dielectronic resonances. A very large energy density of the former would then explain why individual resonances could not be observed experimentally,

Gribakin *et al* (1999) also proposed that, owing to such complexity, the system could be studied by statistical means. This idea has been developed further by Flambaum *et al* (2002). To explain their method, let us adopt a perturbation theory approach. The initial state of the recombination process contains an electron with energy $\varepsilon > 0$ moving in the field of a target ion in the ground state. The latter is usually simple and is dominated by a particular electron configuration. Due to the electron Coulomb interaction, the incident electron may become captured by exchanging energy and exciting one of the target electrons, thereby forming a doubly excited state with the energy $\varepsilon_\alpha + \varepsilon_\beta - \varepsilon_\gamma$. Here α and β are the orbitals occupied by the two electrons and γ is the parent orbital of the excited electron, occupied in the target ground state. So far this picture is identical to that of DR, with a resonance at $\varepsilon \approx \varepsilon_\alpha + \varepsilon_\beta - \varepsilon_\gamma$. However, in a system characterized by a large density of excited states and strong configuration mixing, a simple dielectronic excitation does not constitute an eigenstate. Instead, it is mixed with other more complicated (multiply excited) configurations which cannot be populated directly from the initial state. As a result, the dielectronic configuration plays the role of a *doorway* for the electron capture process. This is shown schematically in figure 1.

The method developed by Flambaum *et al* (2002) is based on the assumption of strong configuration mixing. It allows one to calculate the energy-averaged capture cross section as a sum over the doorway states and to avoid diagonalization of very large configuration-interaction (CI) Hamiltonian matrices. In the case of electron recombination with Au^{25+} the size of the effective Hilbert space is so large that such diagonalization is hardly possible (Gribakin *et al* 1999). Moreover, it is not needed, because the experiment does not resolve particular resonances, and only energy-averaged quantities are measured.

It should be noted that the energy-averaged capture cross section in the method of Flambaum *et al* depends weakly (through Γ) on the strength of mixing between the dielectronic doorways and other multiply excited states. However, if the mixing is strong, the autoionization widths of the doorways (which determine the size of the capture cross section) are shared between a large number of complex multiply excited states. This makes the autoionization widths of the corresponding resonances small. On the other hand, their radiative widths are not suppressed, which results in fluorescence yields close to unity and explains the high recombination rate of Au^{25+} . On the quantitative side, the calculations of Flambaum *et al* (2002) reproduce the observed recombination rates at $\varepsilon \sim 1$ eV.

In the present paper we verify the main assumption of the statistical theory about mixing between the doorway configurations and more complicated excited states of Au^{24+} . We also want to establish the magnitude of the spreading width. Another aim is to test whether the state mixing in this system has indeed reached its ultimate form termed *many-body quantum chaos* (Flambaum *et al* 1994, 1999, Zelevinsky *et al* 1996). In this regime the configuration-based basis states are mixed completely (within the energy range Γ) and the eigenstates lack any ‘individual features’. Such states do not possess any good quantum numbers except the exact ones: energy, parity and the total angular momentum, and their components fluctuate similarly to those of eigenstates of random matrices.

To achieve our goals we perform a detailed numerical study of the chaotic nature of dielectronic doorways and other multiply excited states, keeping in mind that such states are behind the enhancement of low-energy electron recombination with Au^{25+} and similar complex multicharged ions.

2. The compound ion: Au^{24+}

Electron recombination with Au^{25+} results in the formation of Au^{24+} . This ion has 55 electrons and its ground state belongs to the $1s^2 \dots 4d^{10}4f^9$ configuration. To determine its ionization potential we start from a self-consistent relativistic Hartree–Fock calculation of $\text{Au}^{24+} 4f^9$. A CI calculation, which includes all relativistic $4f^9$ configurations, shows that the Au^{24+} ground state is characterized by the total angular momentum $J = \frac{15}{2}$ and total energy $E_{\text{tot}} = -18\,792.485$ au. A similar calculation for the $J = 6$ ground state of $\text{Au}^{25+} 4f^8$, where the Hartree–Fock basis is optimized for the $4f^8$ configuration, gave $E_{\text{tot}} = -18\,764.804$ au. This yields the ionization potential of $I = 27.68$ au = 753.2 eV, slightly higher than $I = 27.56$ au reported in Gribakin *et al* (1999). The latter value was obtained by using the same set of orbitals from the $4f^8$ Hartree–Fock basis in the CI calculations of both ionic ground states ($E_{\text{tot}} = -18\,792.359$ au for Au^{24+}).

In this work we are interested in multiply excited states of Au^{24+} near its ionization threshold. A set of excited single-electron orbitals nlj ($5s_{1/2}$, $5p_{1/2}$, $5p_{3/2}$, etc, up to $7g_{9/2}$) was obtained from a relativistic Hartree–Fock calculation in the self-consistent field of the frozen $\text{Au}^{25+} 1s^2 \dots 4f^8$ residue. For the purpose of our study, Au^{24+} is considered as a system of 19 active electrons above the frozen Kr-like core, $E_{\text{core}} = -17\,822.262$ au. The $4p$ orbitals are sufficiently deep ($\epsilon_{4p_{1/2}} = -49.1$ au and $\epsilon_{4p_{3/2}} = -45.2$ au in Au^{24+} , see Gribakin *et al* (1999) or Flambaum *et al* (2002) for the single-electron energy level diagram) and can be regarded as inactive. Excited state configurations are obtained by distributing the 19 electrons among 31 relativistic orbitals from $4d_{3/2}$ to $7g_{9/2}$. The basic structure of the excitation spectrum of Au^{24+} is found by calculating the energies of the configurations in the mean-field approximation:

$$E_c = E_{\text{core}} + \sum_a \epsilon_a n_a + \sum_{a < b} \frac{n_a(n_b - \delta_{ab})}{1 + \delta_{ab}} U_{ab}, \quad (1)$$

and evaluating the numbers of many-electron states N_c in each configuration:

$$N_c = \prod_a \frac{g_a!}{n_a!(g_a - n_a)!}, \quad (2)$$

where n_a are the orbital occupation numbers of the relativistic orbitals in a given configuration, so that $\sum_a n_a = n$ is the total number of active electrons, i.e. 19. In the equations above, $\epsilon_a = \langle a | H_{\text{core}} | a \rangle$ is the single-particle energy of orbital a in the field of the core, $g_a = 2j_a + 1$, and U_{ab} is the average Coulomb matrix element for the electrons in orbitals a and b (direct

minus exchange):

$$U_{ab} = \frac{g_a}{g_a - \delta_{ab}} \left[R_{abab}^{(0)} - \sum_{\lambda} \delta_p R_{abba}^{(\lambda)} \begin{pmatrix} j_a & j_b & \lambda \\ \frac{1}{2} & -\frac{1}{2} & 0 \end{pmatrix}^2 \right], \quad (3)$$

where $R_{abba}^{(\lambda)}$ is the two-body radial Coulomb integral of multipole λ , and $\delta_p = 1$ when $l_a + l_b + \lambda$ is even and 0 otherwise. In section 3 we show that the mean energies obtained from equation (1) are close to the accurate configuration averages. Even the CI ground state of Au^{24+} is only 0.28 au below the mean energy of the lowest configuration $4d_{3/2}^4 4d_{5/2}^6 4f_{5/2}^6 4f_{7/2}^3$ obtained from equation (1).

A computation slightly more involved than equation (2) allows us to calculate the range of the total angular momenta J and the numbers of energy levels $N_c^{(J)}$ for each J , in each of the configurations, $\sum_J (2J + 1) N_c^{(J)} = N_c$. It turns out that for the configurations close to the ionization threshold of Au^{24+} , $J = \frac{9}{2}$ is the most abundant value (see the inset to figure 2 in Gribakin *et al* (1999)).

Using equations (1)–(3) we have generated a list of about 19 000 configurations with energies within 40 au of the Au^{24+} ground state. Of these configurations, 1158 even and 1323 odd configurations have energies below the ionization threshold of Au^{24+} . They comprise a total of 1.01×10^7 even and 1.43×10^7 odd many-electron states. Our study focuses on the configurations near the ionization threshold. We find 609 even configurations (1.24×10^7 states) and 298 odd configurations (2.56×10^6 states) within 1 au of the threshold.

These large numbers are the result of: (i) the open-shell nature of Au^{24+} and (ii) the ‘gapless’ single-particle excitation spectrum of this ion. The latter also leads to a characteristic exponential growth of the level density with the excitation energy E , $\rho(E) \simeq A E^{-\nu} \exp(a\sqrt{E})$, where $A = 31.6$, $\nu = 1.56$ and $a = 3.35$ (Gribakin *et al* 1999). Given that the excited state configurations cover a whole range of angular momenta J (about 10), and taking into account the $2J + 1$ degeneracy, it is easy to estimate that the mean level spacing between the J^π eigenstates at $E \approx I$ is about 1 meV.

This number does not contain much information about the structure of the eigenstates. In particular, one needs to know whether they are dominated by single configurations, or if a strong configuration mixing is involved. This question can be answered by performing a multiconfigurational CI calculation. In our case, however, the number of configurations is so large, and the configurations are so rich, that this becomes virtually an impossible task.

3. Configuration mixing in Au^{24+}

Earlier limited CI calculations which included just two multiply excited configurations, $4f_{5/2}^3 4f_{7/2}^3 5p_{1/2} 5p_{3/2} 5g_{7/2}$ and $4f_{5/2}^3 4f_{7/2}^3 5p_{1/2} 5d_{3/2} 5f_{7/2}$, pointed towards an extremely strong configuration mixing (Gribakin *et al* 1999). In such situations each eigenstate $|\Psi\rangle = \sum_j C_j |\Phi_j\rangle$, expressed as a linear combination of configuration basis states $|\Phi_j\rangle$, contains a large number N of *principal* components for which $C_j \sim 1/\sqrt{N}$ (recall the normalization condition $\sum_j |C_j|^2 = 1$). This number is estimated by $N \sim \Gamma/D$, where the spreading width Γ is related to the eigenvalue density ρ and the mean-squared value of the off-diagonal Hamiltonian matrix element H_{ij} by means of a golden-rule type formula: $\Gamma = 2\pi |H_{ij}|^2 \rho$. The principal components correspond to the basis states j whose energies are close to the eigenvalue E , $|E_j - E| \lesssim \Gamma$. Distant basis states for which $|E_j - E| \gg \Gamma$ are characterized by small contributions. The mean-squared component $\overline{|C_j|^2}$ is a smooth function of $E_j - E$, well approximated by a Breit–Wigner (BW) formula, while for fixed $E_j - E$ the statistics of C_j are close to Gaussian (see, e.g., Flambaum *et al* 1994).

In this case the eigenvalue spectrum displays so-called level repulsion effects, as small level spacings are infrequent and the probability density of normalized level spacings is close to the Wigner–Dyson ansatz (see, e.g., Bohr and Mottelson 1969):

$$P(S) = (\pi S/2) \exp(-\pi S^2/4). \quad (4)$$

This formula describes level statistics for Hamiltonians modelled by random matrices. Studies of experimental spectra of heavy nuclei (Bohr and Mottelson 1969) and complex atoms and ions (Rosenzweig and Porter 1960, Camarda and Georgopoulos 1983) agree with the Wigner–Dyson statistics. Similar level repulsion effects and statistics of level spacings were also observed in calculations for the cerium atom (Flambaum *et al* 1994, 1998, 1999) and in the nuclear s–d shell model (Horoi *et al* 1995, Frazier *et al* 1996, Zelevinsky *et al* 1995, 1996). These works show that this and other features of the spectrum and eigenstates allow one to speak of many-body quantum chaos. In particular, equation (4) holds only if all states in a manifold ‘interact’, i.e. there are no extra quantum numbers which distinguish them and prevent mixing.

In what follows we present a systematic analysis of these features in the spectrum of doubly and multiply excited states of Au²⁴⁺.

3.1. Statistical features of the spectrum

In the paper by Flambaum *et al* (2002) the recombination cross section of Au²⁵⁺ at low (eV) electron energy was calculated as a sum over the dielectronic doorway states. They assumed that the target ground state is described by the 4d_{3/2}⁴4d_{5/2}⁶4f_{5/2}⁶4f_{7/2}² configuration. This is a reasonable approximation, given that in a CI calculation of the Au²⁵⁺ ground state, which includes all relativistic 4f⁸ configurations, the mean occupation numbers of the 4f_{5/2} and 4f_{7/2} orbitals are 4.93 and 3.07, respectively. Flambaum *et al* (2002) presented a list of important doorways, i.e. those which give large contributions to the cross section. We begin by studying configuration mixing between these doorways.

Most of the doorway configurations in table 1 of Flambaum *et al* (2002) are even. In fact, the density of even multiply excited states is about five times that of the odd states near the ionization threshold of Au²⁴⁺ (see section 2), so we focus on the even states here. Of the 11 even doorway states, let us first consider those 6 which belong to the 4d¹⁰4f⁷5f5g configuration (see table 1). Note that the energies of configurations and eigenstates in the table and below are given with respect to the Au²⁴⁺ ground state in the 4f⁸ basis, for which the ionization threshold of Au²⁴⁺ is at $E = I = 27.56$ au.

To analyse the mixing between the doorway states, we first perform a CI calculation for the doorway configurations 1–6, which produces a total of 316 $J = \frac{9}{2}$ levels. This value of the total angular momentum is the most abundant of all J , which range from $\frac{1}{2}$ to $\frac{35}{2}$. To investigate the effect of mixing of the doorways with more complicated configurations, we have performed three other CI calculations of increasing size. Besides the 6 doorways, they include configurations 7 and 8 (a total of 893 $J = \frac{9}{2}$ levels), configurations 8–11 (2091 levels) and configurations 8–13 (3076 levels). All of the configurations lie close to the ionization threshold. Table 1 lists the configurations, their mean energies, total numbers of states in each configuration and the numbers of states with $J = \frac{9}{2}$. The mean energies E_c obtained from equation (1) are close to those found by averaging over the J subspace of configuration c , $\bar{E}_c = \sum_{i \in c} H_{ii}^{(J)} / N_c^{(J)}$, where $H_{ii}^{(J)}$ are the diagonal Hamiltonian matrix elements in the J subspace. This proximity means that the simple mean-field approach (1) is a reliable tool for finding configurations in a given energy range.

For an overview of the spectra of eigenvalues $E^{(i)}$ obtained in each of the four CI calculations, figure 2 displays the cumulative number of levels:

Table 1. 5f5g doorways and multiply excited configurations of Au²⁴⁺.

No	Doorway configurations from Flambaum <i>et al</i> (2002)	E_c^a (au)	\bar{E}_c^b (au)	N_c	$N_c^{(J)}$
1	4d _{3/2} ⁴ 4d _{5/2} ⁶ 4f _{5/2} ⁶ 4f _{7/2} 5f _{5/2} 5g _{7/2}	27.367	27.397	384	6
2	4d _{3/2} ⁴ 4d _{5/2} ⁶ 4f _{5/2} ⁵ 4f _{7/2} ² 5f _{5/2} 5g _{7/2}	27.742	27.782	8 064	90
3	4d _{3/2} ⁴ 4d _{5/2} ⁶ 4f _{5/2} ⁶ 4f _{7/2} 5f _{7/2} 5g _{7/2}	27.565	27.581	512	7
4	4d _{3/2} ⁴ 4d _{5/2} ⁶ 4f _{5/2} ⁶ 4f _{7/2} 5f _{7/2} 5g _{9/2}	27.629	27.721	640	8
5	4d _{3/2} ⁴ 4d _{5/2} ⁶ 4f _{5/2} ⁵ 4f _{7/2} ² 5f _{7/2} 5g _{7/2}	27.905	27.944	10 752	108
6	4d _{3/2} ⁴ 4d _{5/2} ⁶ 4f _{5/2} ⁵ 4f _{7/2} ² 5f _{5/2} 5g _{9/2}	27.846	27.892	10 080	97
Other configurations					
7	4d _{3/2} ⁴ 4d _{5/2} ⁶ 4f _{5/2} ⁵ 4f _{7/2} ² 5f _{7/2} 5g _{9/2}	27.939	27.981	13 440	117
8	4d _{3/2} ⁴ 4d _{5/2} ⁶ 4f _{5/2} ⁴ 4f _{7/2} ³ 5f _{7/2} 5g _{7/2}	28.182	28.252	53 760	460
9	4d _{3/2} ⁴ 4d _{5/2} ⁵ 4f _{5/2} ⁵ 4f _{7/2} ³ 5p _{3/2} 5f _{5/2}	27.774	27.897	48 384	519
10	4d _{3/2} ⁴ 4d _{5/2} ⁶ 4f _{5/2} ⁴ 4f _{7/2} ³ 5f _{5/2} 5g _{7/2}	28.054	28.129	40 320	381
11	4d _{3/2} ⁴ 4d _{5/2} ⁶ 4f _{5/2} ⁴ 4f _{7/2} ³ 5f _{5/2} 5g _{9/2}	28.128	28.196	50 400	415
12	4d _{3/2} ⁴ 4d _{5/2} ⁶ 4f _{5/2} ⁴ 4f _{7/2} ³ 5f _{7/2} 5g _{9/2}	28.186	28.286	67 200	507
13	4d _{3/2} ⁴ 4d _{5/2} ⁶ 4f _{5/2} ⁴ 4f _{7/2} ² 5p _{3/2} 5d _{3/2} 5f _{5/2}	28.428	28.478	40 320	478

^a E_c is the configuration energy (1) and N_c is the total number of states (2).

^b \bar{E}_c is the average configuration energy in the J subspace and $N_c^{(J)}$ is the number of energy levels with a given J ($=\frac{9}{2}$).

$$N(E) = \int_{-\infty}^E \rho(E') dE', \tag{5}$$

where $\rho(E) = \sum_i \delta(E - E^{(i)})$ is the eigenvalue density for $J^\pi = \frac{9}{2}^+$. The scale of figure 2 makes it impossible to see that $N(E)$ are, in fact, discontinuous step-like functions. When the level mixing is strong the spectra have only a small proportion of small spacing (due to level repulsion) and virtually no large spacings, and are ‘rigid’. It may be seen that our spectra have a high degree of rigidity and it is the configuration mixing that makes them so smooth and uniform.

In all four cases the level density is fitted accurately by a Gaussian function with the skewness (κ_1) and excess (κ_2) corrections:

$$\rho(E) = N_J \frac{\exp(-x^2/2)}{\sqrt{2\pi}\sigma} \left[1 + \frac{\kappa_1}{6}(x^3 - 3x) + \frac{\kappa_2}{24}(x^4 - 6x^2 + 3) \right] \tag{6}$$

where N_J is the number of levels in the spectrum, $x = (E - \bar{E})/\sigma$ is a dimensionless variable, $\bar{E} = N_J^{-1} \sum_i E^{(i)}$ is the mean energy of the manifold, $\sigma^2 = N_J^{-1} \sum_i (E^{(i)} - \bar{E})^2$ characterizes the width of the spectrum, while $\kappa_1 = N_J^{-1} \sum_i (E^{(i)} - \bar{E})^3/\sigma^3$ and $\kappa_2 = N_J^{-1} \sum_i (E^{(i)} - \bar{E})^4/\sigma^4 - 3$ are determined by the third and fourth moments of the eigenvalue distribution, respectively (see, e.g., Ratcliff 1971, Karazija 1991). Parameters of the fits for the four sets of CI calculations are given in table 2.

Using the density fit (6) we test the statistics of the normalized nearest-neighbour level spacings $S_i = (E^{(i+1)} - E^{(i)})\rho(E^{(i)})$ for each of the spectra. Figure 3 shows that the distribution of the spacings is in agreement with the Wigner–Dyson formula (4), which provides evidence of strong level mixing both within and between the configurations. Such mixing also manifests in long-range correlations between the eigenvalues. For example, one could examine the

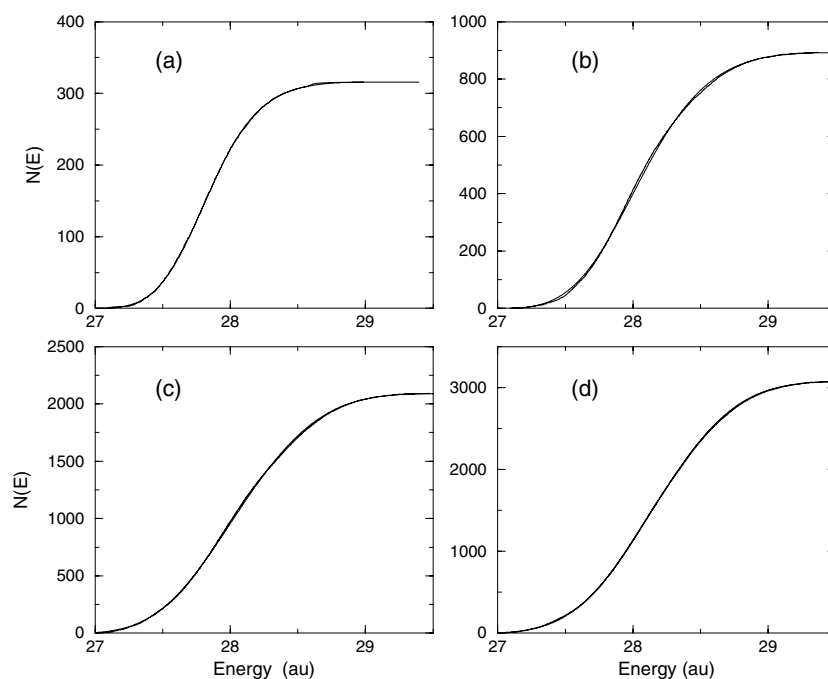


Figure 2. Eigenvalue spectra from CI calculations of $J^\pi = \frac{9}{2}^+$ levels: (a) 316 states, (b) 893 states, (c) 2091 states and (d) 3076 states. The step-like graphs of $N(E)$ are almost indistinguishable, except in (b), from the smooth curves obtained by fitting the level density with equation (6) using parameters from table 2.

Table 2. Parameters of the level densities.

N_J	\bar{E}	σ	κ_1	κ_2
316	27.858	0.308	0.411	0.178
893	28.081	0.396	0.410	-0.096
2091	28.071	0.451	0.231	-0.369
3076	28.169	0.455	0.135	-0.285

uniformity (or rigidity) of the spectrum by studying the Dyson–Mehta Δ_3 statistic (Dyson and Mehta 1963):

$$\Delta_3(L) = \frac{1}{L} \left\langle \min(A, B) \int_E^{E+L} [N(E') - AE' - B]^2 dE' \right\rangle, \quad (7)$$

where the averaging on the right-hand side is over E . This statistic is often used to study level spectra fluctuations (see, e.g., Camarda and Georgopoulos 1983). However, with the electron recombination problem in mind, it is more instructive to examine the structure of the eigenstates.

3.2. Eigenstate components

As mentioned at the beginning of section 3, in the regime of strong configuration mixing, the eigenstate components C_j have the statistics of Gaussian random variables. At the same time the behaviour of the mean-squared components $\overline{|C_j|^2}$ as a function of the basis state energy is

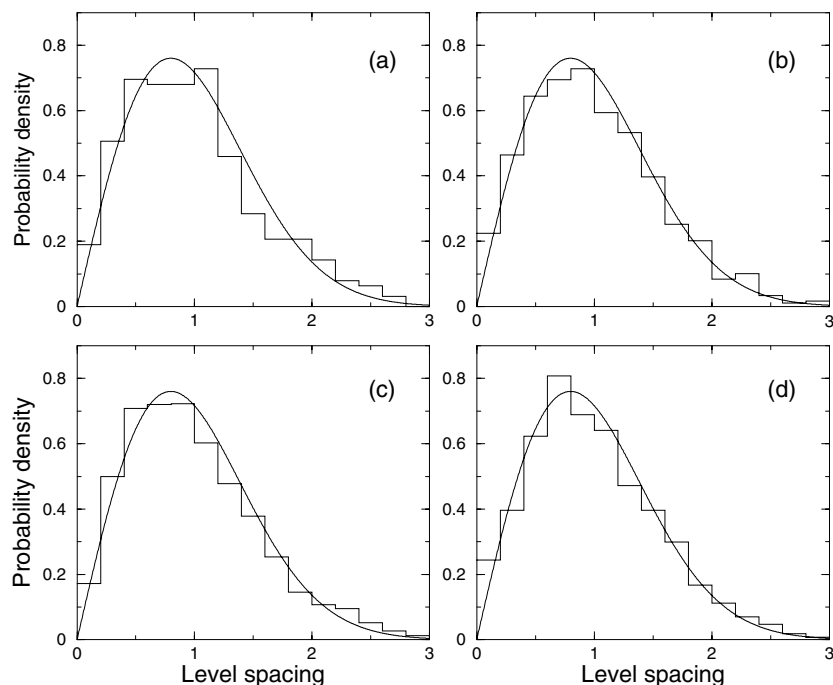


Figure 3. Comparison of the statistics of normalized level spacings obtained in the CI calculations (histograms) with the Wigner–Dyson distribution (4) (full curves): (a) 316 states, (b) 893 states, (c) 2091 states and (d) 3076 states.

described by the BW formula

$$\overline{|C_j|^2} = \frac{1}{N} \frac{\Gamma^2/4}{(E_j - E)^2 + \Gamma^2/4}, \quad (8)$$

where E is the energy eigenvalue. In a random matrix model the averaging of $|C_j|^2$ is performed over an ensemble of random Hamiltonian matrices. When dealing with a real system, we have a unique Hamiltonian matrix. So, the averaging can be done over a number of components falling within fixed narrow bins on the energy scale, and also over a number of neighbouring eigenstates. Equation (8) gives a precise definition of the number of principal components N : $\overline{|C_j|^2}_{\max} = N^{-1}$. The normalization condition links it to the mean level spacing and the spreading width by $N = \pi\Gamma/2D$.

In figure 4 we present the mean-squared components for the $J^\pi = \frac{9}{2}^+$ eigenstates from the middle of the spectra of the four CI calculations. Values of $\overline{|C_j|^2}$, shown as histograms, are obtained by bin averaging the squared components over 19 neighbouring eigenstates in each case. Their energy dependence is in good agreement with the BW profile, except at the edges of the spectrum. In each case the BW fit of $\overline{|C_j|^2}$ yields the number of principal components and the spreading width, see table 3.

Note that the spreading width changes little between the four calculations, although the size of the Hamiltonian matrix, N_J , varies by a factor of ten. On the other hand, the number of principal components increases in proportion to N_J . By means of the normalization condition, $N = \pi\Gamma/2D = (\pi\Gamma/2)\rho$, the growth of N can be related to the increase in the level density ρ , which results from adding more configurations within the same energy range.

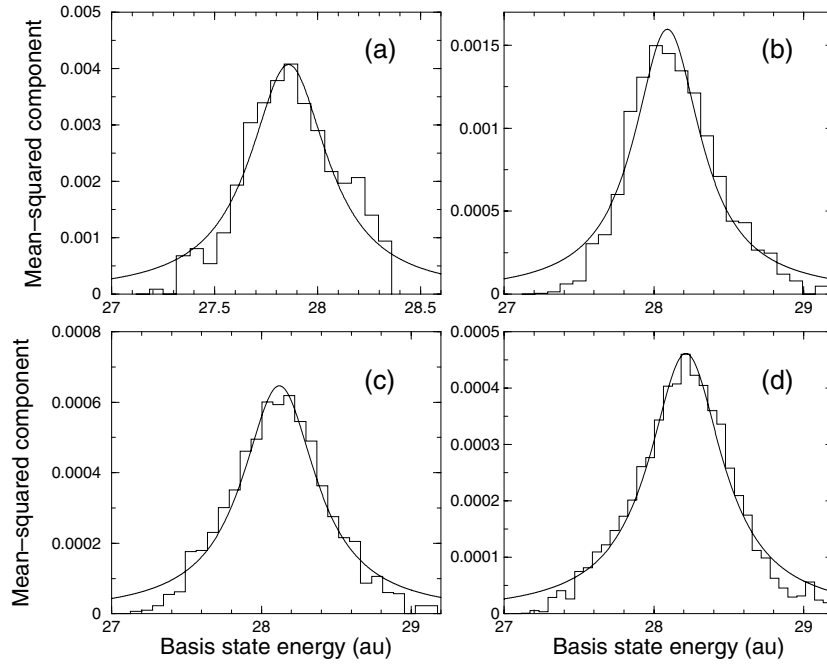


Figure 4. Values of $\overline{|C_j|^2}$ obtained by averaging over 19 neighbouring eigenstates (histograms), and BW fits (8) (full curves) for: (a) 158th eigenstate of 316 states, (b) 446th eigenstate of 893 states, (c) 1046th eigenstate of 2091 states and (d) 1538th eigenstate of 3076 states.

Table 3. Parameters of the mean-squared components of the eigenstates.

N_J	Eigenstate	E^a	N^a	Γ^a	$2\pi\overline{ H_{ij} ^2}\rho$
316	158	27.86	246	0.46	0.46
893	446	28.09	627	0.54	0.50
2091	1046	28.12	1547	0.60	0.70
3076	1538	28.21	2167	0.60	0.62

^a Values determined by fitting numerical $\overline{|C_j|^2}$ by the BW formula (8).

Using the parameters of the BW fit we can extract the densities as $\rho = D^{-1} = 2N/\pi\Gamma$. Combined with the mean squared values of the off-diagonal Hamiltonian matrix elements in the J subspace, $\overline{|H_{ij}|^2}$ (table 4), they provide golden-rule values of the spreading width, $\Gamma = 2\pi\overline{|H_{ij}|^2}\rho$. Table 3 shows that the latter are close to the spreading widths obtained from the eigenstates in figure 4. This is a useful consistency check for the picture of strong (complete, chaotic) basis-state mixing within the eigenstates.

To examine the evolution of the eigenstate shapes $\overline{|C_j|^2}$ across the whole spectrum, in figure 5 we present them for the 300th, 600th, etc, eigenstates of the largest CI calculation ($N_J = 3076$). Features to notice here are the following.

- (i) The spreading width remains almost constant.
- (ii) The bell-shaped $\overline{|C_j|^2}$ is centred on the energy eigenvalue, and is shifted with it as the energy increases. There is also a small outward displacement of the eigenvalue from the peak of $\overline{|C_j|^2}$ noticeable for the states at the edges of the spectrum. This is a consequence

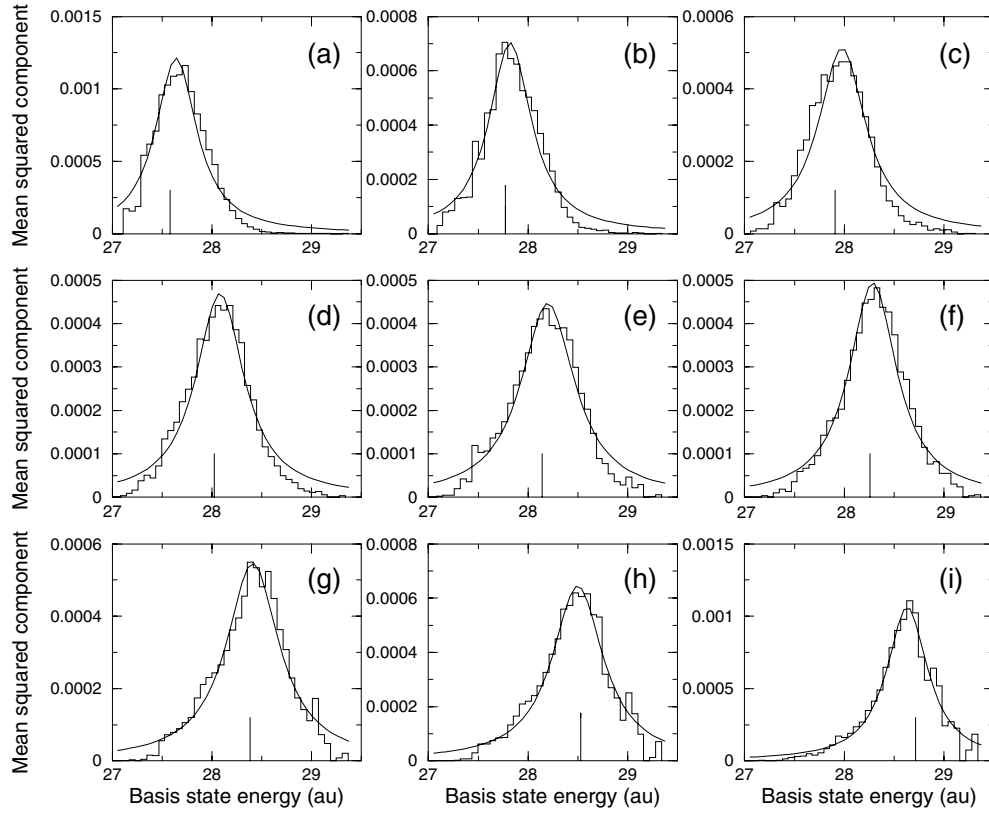


Figure 5. Mean squared components $\overline{|C_j|^2}$ for a number of eigenstates of the $N_J = 3076$ CI calculation. Histograms show numerical values obtained by bin averaging over 19 neighbouring eigenstates for (a) 300th state, (b) 600th state, (c) 900th state, (d) 1200th state, (e) 1500th state, (f) 1800th state, (g) 2100th state, (h) 2400th state and (i) 2700th state. Full curves are BW fits. Vertical bars indicate positions of the corresponding energy eigenvalues.

Table 4. Statistical characteristics of the eigenstates near the middle of the spectrum in each of the four CI calculations.

N_J	IPR ^a	$N/3^b$	$\rho(\bar{E})^c$ (au)	$\overline{ H_{ij} ^2}$ (au)	$2\pi \overline{ H_{ij} ^2} \rho(\bar{E})$ (au)	Γ^d (au)
316	85	82	418	2.14×10^{-4}	0.56	0.44
893	245	211	888	1.08×10^{-4}	0.60	0.57
2091	513	487	1765	6.81×10^{-5}	0.75	0.62
3076	777	715	2603	4.27×10^{-5}	0.70	0.60

^a Maximal window-averaged IPR.

^b Derived from the *maximal* number of principal components N .

^c Eigenvalue density at $E = \bar{E}$ from fit (6).

^d Spreading width from BW fits averaged over the middle 30% of eigenstates.

of level repulsion and overall broadening of the eigenvalue spectrum in comparison with that of basis state energies, due to the off-diagonal Hamiltonian matrix elements.

(iii) The peak values of $\overline{|C_j|^2}$ are larger for the eigenstates near the edges of the spectrum.

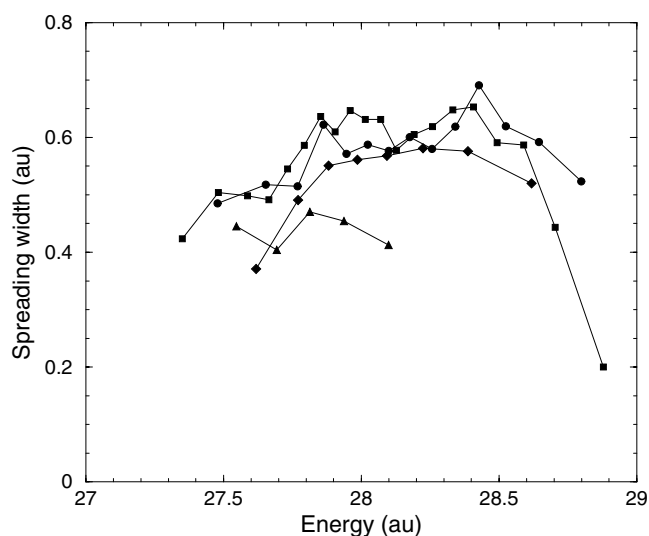


Figure 6. Dependence of the spreading width Γ on the eigenstate energy in the four CI calculations: triangles— $N_J = 316$, diamonds— $N_J = 316$, circles— $N_J = 2091$ and squares— $N_J = 3076$.

As seen from equation (8), this means smaller N , which correlates with smaller level densities at the edges.

Figure 6 shows the dependence of the spreading width on the eigenstate energy in each of the four CI calculations. It was obtained by performing BW fits of the mean squared components for a number of eigenstates across the spectra (e.g. 50th, 100th, 150th, 200th and 250th, for the smallest $N_J = 316$). Most importantly, the spreading widths from the calculations of different sizes have similar magnitudes. They also remain relatively flat over the whole energy range. The drop towards the edges is not a physical feature but a consequence of the limited (and relatively small) number of configurations included in the calculations. The magnitude of Γ remains close to 0.5 au, a value that was originally obtained for Au^{24+} (Gribakin *et al* 1999) based on the study of just two large configurations (see the beginning of section 3). This value is only about five times greater than the spreading width in the neutral atom of Ce (Flambaum *et al* 1994). This is in contrast with the very different energy scales involved—the ionization potentials of Au^{24+} and Ce differ by two orders of magnitude. All these features reflect the nature of the spreading width as a robust characteristic of level mixing in a system.

Large numbers of principal components N in table 3 signify that the eigenstates examined contain sizeable contributions of *many* basis states. A direct measure of the degree of basis-state mixing, which is not related to any particular shape of $|C_j|^2$, is the inverse participation ratio (IPR), $\xi = (\sum_j |C_j|^4)^{-1}$. This quantity can be calculated for each of the eigenstates and is a standard tool for studying eigenstate complexity. In particular, if an eigenstate is a uniform mixture of N components with Gaussian statistics (as that of the Gaussian orthogonal ensemble, see, e.g., Brody *et al* (1981)), then $\overline{|C_j|^2} = N^{-1}$, $\overline{|C_j|^4} = 3(\overline{|C_j|^2})^2$ and $\xi = N/3$.

In figure 7 we plot the IPRs of the eigenstates as a function of their energy. The main feature of the ‘raw’ IPR values in (a), (c), (e) and (g) is their regular dependence on the energy combined with relatively small level-to-level fluctuations. It confirms that the basis-state mixing is practically *complete*, i.e. no particular configurations or basis states escape

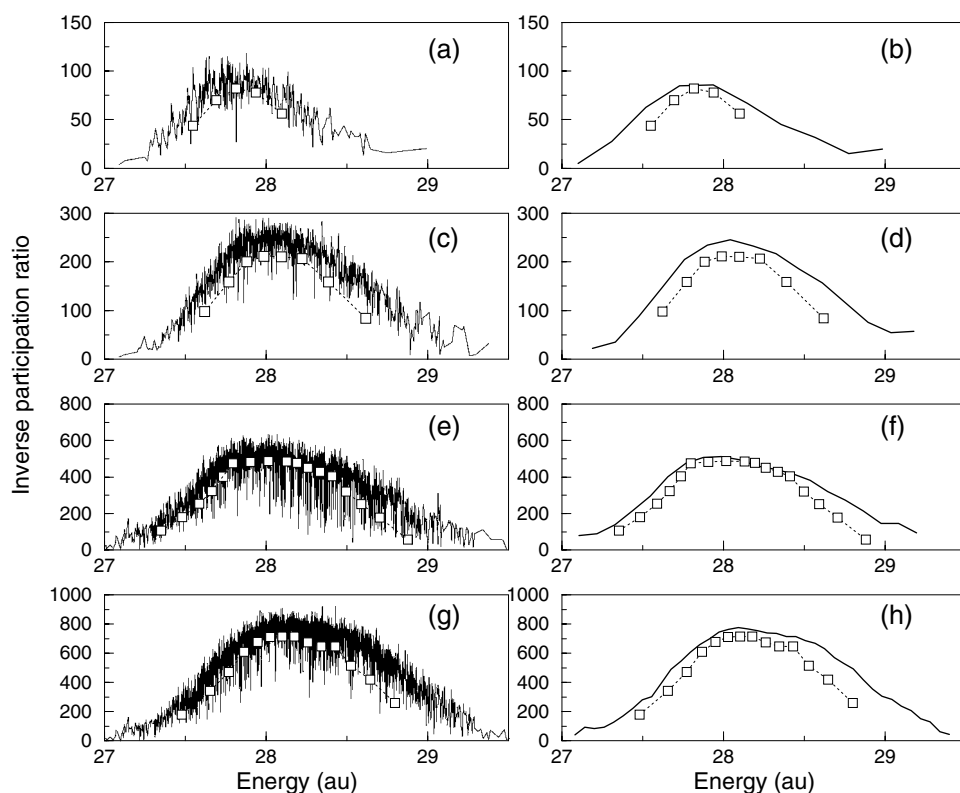


Figure 7. IPRs of the eigenstates as a function of their energy: (a) and (b)—CI with 316 states, (c) and (d)—893 states, (e) and (f)—2091 states, (g) and (h)—3076 states. Thin full curves in (a), (c), (e) and (g) connect the IPRs for all eigenstates, and thick full curves in (b), (d), (f) and (h) show window-averaged IPRs. Open squares show values of $N/3$, with N obtained from BW fitting of $\overline{|C_j|^2}$.

mixing with the rest of the manifold. (If they did this would manifest in a large scatter of IPR values over a narrow energy interval.) Both the IPR and the number of principal components N measure the complexity of the eigenstates. Plots on the right-hand side of figure 7 show that the values of $N/3$ are close to the IPR, as expected if the statistics of the eigenstate components were Gaussian (see the appendix for a detailed discussion). Both quantities peak near the middle of the spectrum where the level density is largest. Peak values of the IPR and $N/3$ in each of the four calculations are shown in table 4.

A picture of typical chaotic eigenstates can be found in Flambaum *et al* (1994) for the neutral Ce atom, or in Gribakin *et al* (1999) for Au^{25+} . Apart from the systematic variation of the magnitudes of C_j with the distance between E_j and eigenvalue E , which is represented by $\overline{|C_j|^2}$ (figures 4 and 5), the components display strong fluctuations. To analyse these, we eliminate the systematic variation of the size of C_j by using *normalized* eigenstate components $C_j[\overline{|C_j|^2}]^{-1/2}$. Their statistics are presented in figure 8 for the same eigenstates that were used to construct $\overline{|C_j|^2}$ in figure 4. The fact that these statistics are so close to Gaussian is another confirmation of complete basis state mixing. If there were configurations which did not participate in the mixing (e.g. because of some hidden selection rules or for some dynamical reasons), the distribution would show an abundance of small component values.

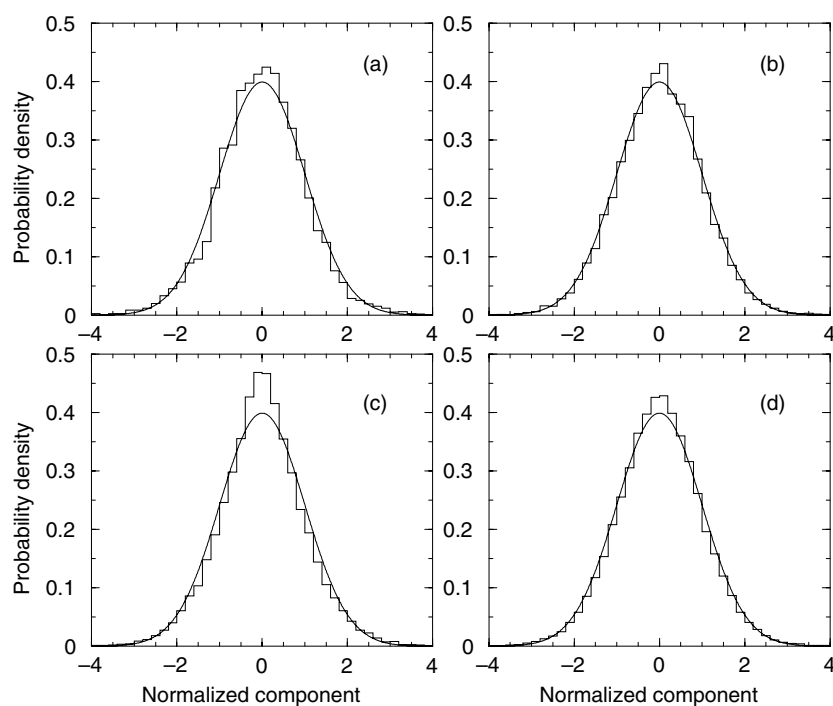


Figure 8. Histograms show statistics of the normalized components $C_j[\overline{|C_j|^2}]^{-1/2}$ for $19 J = \frac{9}{2}^+$ eigenstates from the middle of the spectrum in the CI calculations of four sizes: (a) 316 states, (b) 893 states, (c) 2091 states and (d) 3076 states. Full curves are normal Gaussian distributions.

3.3. Mixing between dielectronic doorways with more complex configurations

So far we have examined the dynamical and statistical properties of configuration mixing in the eigenstates of Au^{24+} . This picture of chaotic complete mixing underpins the statistical approach to the calculation of recombination developed by Gribakin *et al* (1999) and Flambaum *et al* (2002). More specifically, we can now check the assumption that dielectronic states populated at the first step of the capture process (figure 1) are indeed mixed strongly with more complex multiply excited states. To do this we examine the *weights* of large dielectronic (doorway) configurations listed under 2, 5 and 6 in table 1. The weight of a doorway configuration c is defined for each eigenstate as a sum over the basis states belonging to this configuration, $w_c = \sum_{j \in c} |C_j|^2$.

If a doorway configuration does not mix with any other configurations, then its weight in an eigenstate will be either 1 or 0. If, on the contrary, it mixes with them completely then its weight in each of the eigenstates must be close to the mean weight $\bar{w}_c = N_c^{(J)}/N_J$, a fraction of the Hilbert space occupied by the doorway. Figure 9 shows the weights of the three large doorway configurations for the calculations of increasing size. It is evident that the doorway configurations are shared between all eigenstates. This sharing is not completely uniform, since the doorway configuration energies are lower than those of most other configurations included (table 1), and as a result, the doorways are more prominent in the lower part of the spectrum, where their weights exceed \bar{w}_c . Nevertheless, the main feature of the graphs is that the weights of the doorways in individual eigenstates *decrease* as the size of the Hamiltonian matrix increases. This provides evidence that the doorway states are completely mixed within the chaotic eigenstates containing mostly more complicated multiply excited configurations.

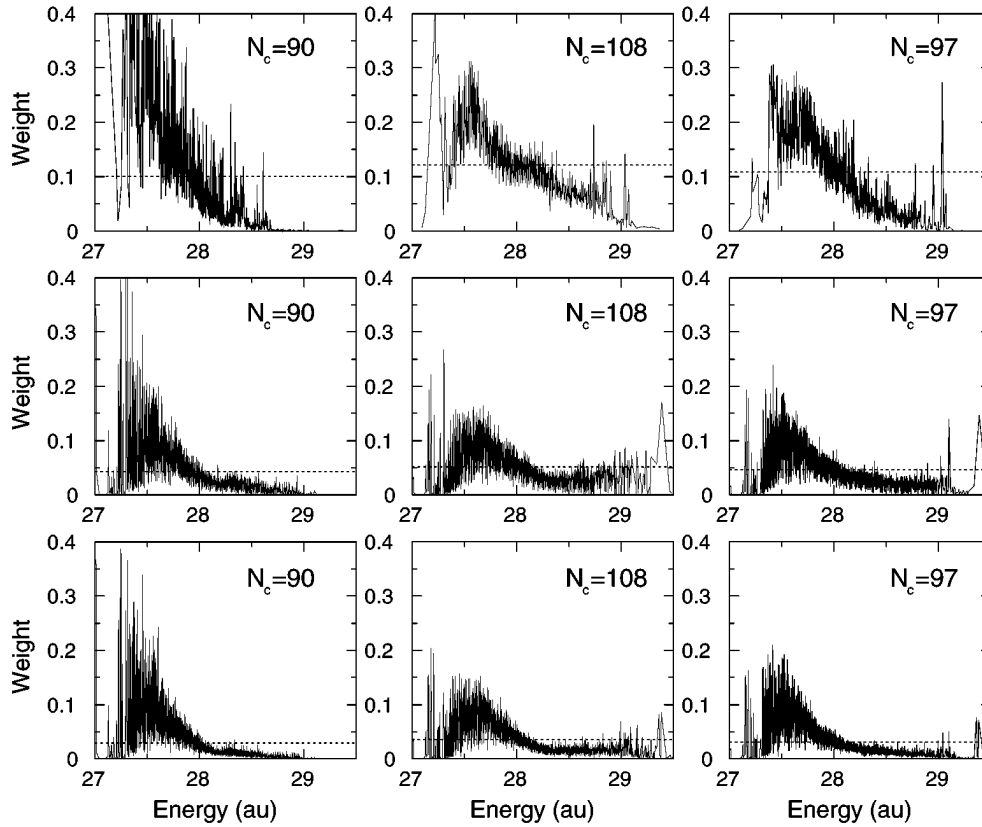


Figure 9. Weights of doorway configurations 2, 3 and 5 from table 1, with 90, 108 and 97 $J^\pi = \frac{9}{2}^+$ states, respectively, in the eigenstates obtained from the CI calculation with $N_J = 893$ states (top row), $N_J = 2091$ (middle row) and $N_J = 3076$ (bottom row). Horizontal dotted lines indicate the mean weights of doorway configurations, \bar{w}_c .

4. Statistical approach and criteria of strong mixing

4.1. Spreading width

Table 4 shows that an increase in the eigenstate complexity in the four calculations, as shown by IPR and N , follows the increase of the level density. At the same time, the spreading width changes little and the golden rule gives a reasonable estimate of Γ (table 3). The latter is an important point.

Even the largest calculation performed includes a relatively small number of configurations in the energy range of interest. According to the estimates of the level density near the ionization threshold of Au^{24+} (section 2), the true mean level spacings for a given J^π can be as small as 10^{-5} au. Given the fact that Γ remains approximately constant, the corresponding eigenstates may contain tens of thousands of principal components $N \sim \Gamma/D$. A straight CI calculation of this size would be very difficult and impracticable, if not altogether impossible. Moreover, its results will be largely meaningless, because in a spectrum of such complexity one will hardly be able to guarantee correct configuration compositions of the individual states.

On the other hand, if the individual eigenstates are not resolved in experiment, one may only be interested in some energy-averaged characteristics of the spectrum and eigenstates,

Table 5. Additional doorway configurations of Au²⁴⁺.

No	Doorway configurations from Flambaum <i>et al</i> (2002)	E_c^a (au)	\bar{E}_c (au)	N_c	$N_c^{(J)}$
1'	$4d_{3/2}^4 4d_{5/2}^5 4f_{5/2}^6 4f_{7/2}^3 7p_{1/2}$	27.465	27.599	672	10
2'	$4d_{3/2}^4 4d_{5/2}^5 4f_{5/2}^6 4f_{7/2}^2 5d_{3/2} 5d_{5/2}$	26.887	26.995	4032	55
3'	$4d_{3/2}^4 4d_{5/2}^5 4f_{5/2}^6 4f_{7/2}^3 6f_{5/2}$	26.585	26.697	2016	26
4'	$4d_{3/2}^4 4d_{5/2}^6 4f_{5/2}^5 4f_{7/2}^2 5d_{5/2} 6f_{5/2}$	27.084	27.112	6048	76
5'	$4d_{3/2}^4 4d_{5/2}^5 4f_{5/2}^6 4f_{7/2}^3 6f_{7/2}$	26.643	26.797	2688	31

^a E_c , \bar{E}_c , N_c and $N_c^{(J)}$ have the same meaning as in table 1, $J = \frac{9}{2}$.

such as the level density, spreading width, number of principal components, etc. Therefore, it is desirable to be able to determine these quantities *without* diagonalizing huge Hamiltonian matrices. Our use of the golden rule to evaluate the spreading width as $\Gamma = 2\pi \overline{|H_{ij}|^2} \rho(\bar{E})$ is an illustration of such an approach. The value of the density at the centre of the spectrum is given by equation (6), $\rho(\bar{E}) \approx N_J (2\pi\sigma^2)^{-1/2}$, where σ is the root-mean-squared width of the eigenvalue spectrum about the mean \bar{E} :

$$\sigma^2 = \frac{1}{N_J} \sum_{ij} H_{ij}^2 - \frac{1}{N_J^2} \left(\sum_i H_{ii} \right)^2 = (N_J - 1) \overline{|H_{ij}|^2} + \frac{1}{N_J} \sum_i (H_{ii} - \bar{E})^2. \quad (9)$$

One could also account for the skewness and excess corrections, since both κ_1 and κ_2 can be expressed in terms of the Hamiltonian matrix elements. The golden-rule formula then gives estimates of the spreading width which are in reasonable agreement with the values obtained from the eigenstate shapes $\overline{|C_j|^2}$, see table 4.

In fact, the golden-rule values are slightly higher in magnitude than those obtained from BW fitting. This can be due to the fact that, for the purpose of fitting, $\overline{|C_j|^2}$ is considered as a function of the *basis state* energy E_j , rather than the energy eigenvalues (see, e.g., figure 5). Because of the level repulsion, the mean spacing between the eigenvalues is greater than that between the basis states. Consequently, the BW spreading width, which must satisfy the normalization condition $\pi\Gamma/2D = N$, appears to be lower.

4.2. Criterion of mixing

As mentioned at the beginning of section 3.1, the CI calculations were performed with six even configurations out of the 11 shown in table 1 of Flambaum *et al* (2002). CI calculations which include the remaining five doorway configurations, listed under 1' to 5' in table 5, show that they do not mix strongly either between themselves, or with other configurations considered above¹.

For example, a calculation which includes all $N_J = 198$ states with $J = \frac{9}{2}$ of the five doorway configurations from table 5 produces a level spacing distribution which does not obey the Wigner–Dyson law, while the IPR of the eigenstates shows large fluctuations, figure 10. The relative weakness and non-uniformity of mixing in this case becomes evident if we compare these graphs with figures 3(a) and 7(a), which illustrate strong mixing of doorway configurations 1–6. Of course, this does not mean that configurations 1'–5' are fundamentally different from 1 to 6. Figure 10(b) does show that most of the eigenstates still contain substantial

¹ In fact, of the doorway configurations 1–6 and 1'–5', only 5 and 4' are directly coupled by the two-body Coulomb interaction.

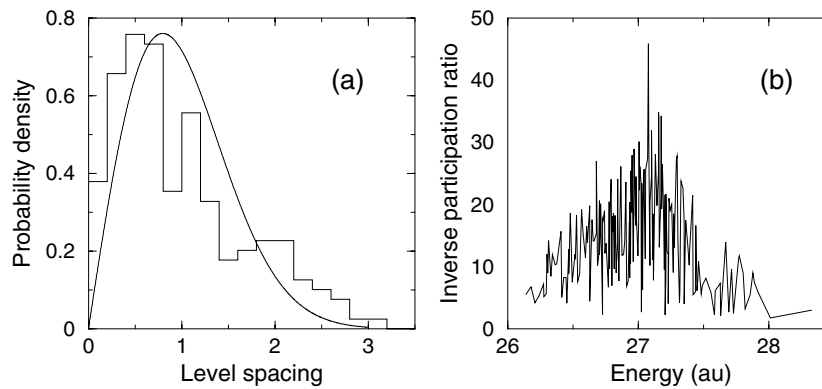


Figure 10. Distribution of normalized level spacings (a) and IPRs (b) of the $J = \frac{9}{2}$ eigenstates obtained in the CI calculation of the doorway configurations 1'–5' (table 5). The full curve in (a) is the Wigner–Dyson ansatz (4).

contributions of many basis-state components. It is also likely that there are multiply excited states which mix strongly with doorways 1'–5'. Such configurations may also promote mixing between the configurations in tables 5 and 1. However, a calculation of this type would require a further increase of the size of the basis and Hamiltonian matrix.

Instead, in this work we would like to understand *why* the mixing between doorways 1'–5' is so different from that of 1–6. More importantly, we put forward a simple estimate which allows one to predict whether a particular set of configurations will exhibit strong mixing, *without* diagonalizing the relevant Hamiltonian matrix. This question is part of a more general problem of finding a criterion of strong chaotic mixing which was addressed in a number of recent papers, see Altshuler *et al* (1997), Jacquod and Shepelyansky (1997), Mirlin and Fyodorov (1997), Flambaum and Izrailev (1997).

The basic result of these works is in agreement with a perturbation-theory argument that two levels i and j mix strongly if the dimensionless ratio

$$\frac{H_{ij}}{E_i - E_j} \quad (10)$$

is of the order of unity or greater and the perturbation series diverges. Applying this idea to configuration mixing, we may compare the root-mean-squared Hamiltonian matrix element V , defined by

$$V^2 = \overline{|H_{ij}|^2} = \frac{1}{N_c^{(J)} N_{c'}^{(J)}} \sum_{i \in c, j \in c'} |H_{ij}|^2, \quad (11)$$

with the typical level spacing ΔE between neighbouring basis states belonging to configurations c and c' . If the two configurations do not overlap on the energy scale, then ΔE is large and determined by the configurations' centroids, $\Delta E \sim |E_c - E_{c'}|$. In this case strong mixing is unlikely, unless V is very large. On the other hand, if we deal with overlapping configurations, then

$$\Delta E = \min\{D_c, D_{c'}\}, \quad (12)$$

where D_c and $D_{c'}$ are the level spacings within the configurations c and c' , which can be small. A simple estimate of these is

Table 6. Parameters of configurations and their mixing for the doorway configurations from table 1.

Conf.	1	2	3	4	5	6
1	27.40 0.105 ^a	0.003 81 1.04 ^b	0.006 48 0.23	0.006 29 0.33	0.000 70 0.24	0.000 52 0.15
2		27.78 0.132	0.006 06 1.65	0 0	0.001 81 0.61	0.001 65 0.47
3			27.58 0.079	0.008 12 0.43	0.003 39 1.15	0 0
4				27.72 0.061	0.003 60 1.22	0.006 46 1.82
5					27.94 0.127	0.006 20 2.10
6						27.89 0.137

^a Diagonal cells show values of E_c and σ_c in atomic units.

^b Off-diagonal cells show values of V in atomic units and dimensionless κ (in bold).

$$D_c \simeq \frac{\sqrt{2\pi}\sigma_c}{N_c^{(J)}}, \quad (13)$$

where σ_c is given by equation (9) with the sums restricted to the basis states within c .

Combining equations (11)–(13), we can estimate the ratio

$$\kappa = \frac{V}{\Delta E}, \quad (14)$$

which should indicate whether the mixing is strong ($\kappa \gtrsim 1$) or weak ($\kappa \ll 1$). Of course, the boundary between the two cases is not sharp, as there is an intermediate regime characterized by ‘non-uniform’ mixing and large non-Gaussian fluctuations. Note that κ is wholly determined by the Hamiltonian matrix elements.

Tables 6 and 7 show, respectively, the six strongly interacting doorway configurations as a 6×6 ‘matrix’ and the five weakly mixed configurations as a 5×5 ‘matrix’. The diagonal cells of each ‘matrix’ contain values of the configuration centroids \bar{E}_c and σ_c for each configuration. The off-diagonal cells show the root-mean-squared Hamiltonian matrix element V for a pair of configurations, together with the mixing parameter κ . Since such ‘matrices’ are symmetric, only the upper triangles are shown.

It is seen from the tables that the mixing strength parameter κ has much larger values for configurations 1–6, many of them close to or greater than unity. On the other hand, all values of κ in table 7 are small, which explains our earlier finding that configurations 1’–5’ do not show strong mixing. It is also instructive to look at figure 11, which shows the positions of the 11 doorway configurations on the energy scale. The bars in the figure correspond to energies from $\bar{E}_c - \sigma_c$ to $\bar{E}_c + \sigma_c$, and show approximately the energy ranges covered by each of the configurations. It is evident that most of the configurations in each of the two sets overlap, e.g. the larger doorways 2, 5 and 6, or 2’ and 4’. Smaller values of κ , however, prevent configurations 1’–5’ from mixing strongly with each other.

As an additional test of the role of the size of V , we boosted the configuration mixing for configurations 1’–5’ by multiplying the corresponding off-diagonal parts of the Hamiltonian matrix by a factor larger than unity. By making it sufficiently large (10 and greater) we did attain the Wigner–Dyson level repulsion features characteristic of the strong mixing regime. The use of such a factor meant that the values of κ in table 7 were artificially increased by an order of magnitude and brought into the range (~ 1) where strong mixing should take place.

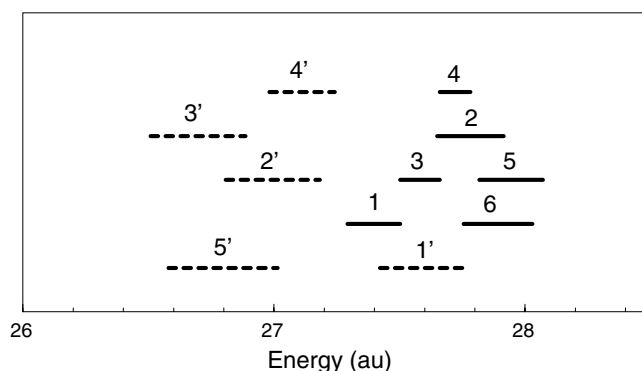


Figure 11. Energy ranges $E_c \pm \sigma_c$ of the doorway configurations 1–6 (full line bars) and 1'–5' (broken line bars).

Table 7. Parameters of configurations and their mixing for the doorway configurations from table 5.

Conf.	1'	2'	3'	4'	5'
1'	27.60	0.000 74	0.001 43	0	0.000 42
	0.177 ^a	0.087^b	0.079	0	0.024
2'		27.00	0.000 11	0.000 75	0.000 15
		0.187	0.013	0.175	0.018
3'			26.70	0.000 47	0.001 43
			0.189	0.110	0.082
4'				27.11	0
				0.130	0
5'					26.80
					0.217

^a Diagonal cells show values of E_c and σ_c in atomic units.

^b Off-diagonal cells show values of V in atomic units and dimensionless κ (in bold).

5. Conclusions

An extensive CI study of doubly and multiply excited states near the ionization threshold of Au^{24+} has confirmed earlier expectations of strong chaotic configuration mixing in this system. As a result of such mixing, 'simple' doubly excited states, which play the role of doorway states in electron–ion recombination, are shared between large numbers of chaotic multiply excited multiconfigurational eigenstates.

The existence of a dense spectrum of such multiply excited states explains the experimental observation of a strongly enhanced but featureless electron recombination rate on Au^{25+} (Hoffknecht *et al* 1998). It is crucial for this phenomenon that sharing of the doorways between multiply excited states leads to small autoionizing widths of the resonances which mediate the process of electron recombination. The small autoionizing widths give rise to large fluorescence yields close to unity (Flambaum *et al* 2002).

Our calculations demonstrate that configuration basis state mixing in Au^{24+} is characterized by the BW shapes of the mean-squared components with the spreading width $\Gamma \sim 0.6$ au and Gaussian statistics of the (normalized) eigenstate components. We have also shown that parameters of the chaotic eigenstates, such as Γ , can be estimated *without* diagonalization of large CI Hamiltonian matrices. In addition, we have shown that one can make conclusions about the degree of configuration mixing by examining a simple

dimensionless parameter κ . It is equal to the ratio of the root-mean-squared Hamiltonian matrix element V between a pair of overlapping configurations to the typical level spacing ΔE : $\kappa = V/\Delta E$. Strong mixing is observed for $\kappa \gtrsim 1$.

A further development of these and similar approaches should lead to a complete statistical theory of Fermi systems with chaotic multiply excited eigenstates, for which a brute force diagonalization of huge Hamiltonian matrices is either very difficult or impossible. The basic ingredients of such a theory are becoming clear now (see Zelevinsky *et al* 1996, Flambaum and Izrailev 1997, Flambaum and Gribakin 2000). There is some similarity between its methods and those of the unresolved transition array formalism and other statistical approaches (see, e.g., Karazija 1991, Bauche *et al* 1988). However, the emerging theory focuses on systems where the transitions are ‘unresolved’ due to strong chaotic level mixing, rather than because of the apparent complexity of the spectra or experimental limitations. In the future this theory should enable one to calculate physical properties of the system averaged over an energy interval containing many chaotic multiply excited eigenstates without diagonalization of the Hamiltonian matrix. Owing to small level spacings, this energy interval can be made small enough to allow useful comparisons with the results of many experiments, including those performed with high energy resolution.

Appendix. Relation between statistics and the shape of components and IPR

There are two main features which characterize the components C_j of a chaotic eigenstate with energy E . The first feature concerns the statistics of the components, which appear to be random or almost random. This behaviour is a consequence of strong mixing and quasi-random Hamiltonian matrix elements in a complex system, which make the components corresponding to different basis states statistically independent².

The second feature is a systematic dependence of the size of the components on the basis state energy $E_j \equiv H_{jj}$. Thus, C_j are typically large for the basis states whose energies are close to E , and small for those j for which $|E_j - E| > \Gamma$, where Γ is the energy width characteristic of the mixing (spreading width). Such behaviour is in agreement with an understanding based on perturbation theory—contributions of distant basis states become smaller as $|E_j - E|$ increases.

A natural way to separate out the systematic and random features of C_j is by calculating locally averaged mean-squared components $\overline{|C_j|^2}$ (for fixed $E_j - E$) and considering the statistics of locally normalized components $C_j(\overline{|C_j|^2})^{-1/2}$, see figures 4, 5 and 8. These figures show that, for the eigenstates studied, this statistic is close to Gaussian, while the shapes are described well by the BW profiles (8), although $\overline{|C_j|^2}$ drops faster at the edges.

Assuming that the statistics of locally normalized components are the same for all $E_j - E$, we can directly relate the IPR to the eigenstate shape and fourth moment of the (locally normalized) components. To do this, we express the fourth moment in terms of the second moment as

$$\overline{|C_j|^4} = A(\overline{|C_j|^2})^2, \quad (\text{A.1})$$

where A depends on the (local) distribution of C_j . Thus, if the fluctuations of C_j are locally Gaussian then $A = 3$. If there is a certain excess of both small and large components, as in figure 8(c), then $A > 3$. The IPR $\xi = \sum_j |C_j|^4$ for an eigenstate with energy E is then found

² Note that in a many-body system there are some correlations between distant components, due to a two-body nature of the interaction between the particles (Flambaum *et al* 1996).

as follows:

$$\xi^{-1} = \sum_j \overline{|C_j|^4} = A \sum_j \overline{(|C_j|^2)^2} \approx A \int [f(E_j)]^2 \frac{dE_j}{D}, \quad (\text{A.2})$$

where we eliminate level-to-level fluctuations of ξ^{-1} by averaging over a number of neighbouring eigenstates and $f(E_j) \equiv \overline{|C_j|^2}$ describes the shape of the eigenstate and is normalized by $\int f(E_j) dE_j/D = 1$.

For a Gaussian orthogonal ensemble where all basis states are equivalent, $f(E_j) = 1/N =$ constant, and $A = 3$, we have $\xi = N/3$. For eigenstates with $f(E_j)$ given by the BW formula (8), equation (A.2) gives $\xi = 2N/A$. A stronger localization of the eigenstate with more rapidly decreasing $\overline{|C_j|^2}$ can be modelled by a Gaussian envelope:

$$\overline{|C_j|^2} \equiv f(E_j) = \frac{1}{N} \exp\left[-\frac{(E_j - E)^2}{2a^2}\right]. \quad (\text{A.3})$$

The normalization condition requires $a = ND/\sqrt{2\pi}$, the full width at half-maximum being $\Gamma = 2a\sqrt{2\ln 2}$, and equation (A.2) yields $\xi = \sqrt{2}N/A$. In all these cases the number of principal components N is defined by $\overline{|C_j|^2}_{\max} = N^{-1}$.

Therefore, we see that, although the IPR and N are proportional to each other, the coefficient can be different, depending on the eigenstate shape $f(E_j)$ and the value of A determined by the local statistical distribution of C_j . If the eigenstates components had accurate BW shapes and exact Gaussian statistics, we would have $\xi = 2N/3$. However, figure 7 shows that values of IPR are close to $N/3$. To understand this discrepancy, we calculate A for the distributions shown in figures 8(a)–(d) and obtain 3.69, 3.54, 3.98 and 3.70, respectively. Using values of $\overline{|C_j|^2}$ from figure 4 (histograms), we evaluate $\int [f(E_j)]^2 \frac{dE_j}{D}$ and obtain 0.67, 0.65, 0.64 and 0.63. These values are between 0.5 and $2^{-1/2} \approx 0.71$, which characterize the BW and Gaussian shapes, respectively. The resulting ratios $N/\xi = 2.47, 2.30, 2.54$ and 2.33 , are smaller than, but close to, 3, in qualitative agreement with figure 7.

References

- Altshuler B L, Gefen Yu, Kamenev A and Levitov S L 1997 *Phys. Rev. Lett.* **78** 2803–6
 Bauche J, Bauche-Arnoult C and Klapisch M 1988 *Adv. At. Mol. Phys.* **23** 131–95
 Bohr A and Mottelson B 1969 *Nuclear Structure* vol 1 (New York: Benjamin)
 Brody T F, Flores J, French J B, Mello P A, Pandey A and Wong S S M 1981 *Rev. Mod. Phys.* **53** 385–479
 Camarda H S and Georgopoulos P D 1983 *Phys. Rev. Lett.* **50** 492–5
 Dyson F and Mehta M L 1963 *J. Math. Phys.* **4** 701
 Flambaum V V and Gribakin G F 2000 *Phil. Mag.* **B 80** 2143–73
 Flambaum V V, Gribakin G F, Gribakina A A and Harabati C 2002 *Phys. Rev. A* **66** 012713
 Flambaum V V, Gribakin G F and Izrailev F M 1996 *Phys. Rev. E* **53** 5729–41
 Flambaum V V, Gribakina A A and Gribakin G F 1998 *Phys. Rev. A* **58** 230–7
 Flambaum V V, Gribakina A A, Gribakin G F and Kozlov M G 1994 *Phys. Rev. A* **50** 267–95
 Flambaum V V, Gribakina A A, Gribakin G F and Ponomarev I V 1999 *Physica D* **131** 205–20
 Flambaum V V and Izrailev F M 1997 *Phys. Rev. E* **55** 5144–59
 Frazier N, Brown B A and Zelevinsky V 1996 *Phys. Rev. C* **54** 1665–74
 Gao H, Schuch R, Zong W, Justiniano E, DeWitt D R, Lebius H and Spies W 1997 *J. Phys. B: At. Mol. Opt. Phys.* **30** L499–506
 Graham W G, Fritsch W, Hahn Y and Tanis J A (ed) 1992 *Recombination of Atomic Ions (NATO ASI Series B: Physics vol 296)* (New York: Plenum)
 Gribakin G F, Gribakina A A and Flambaum V V 1999 *Aust. J. Phys.* **52** 443–57
 Gwinner G et al 2000 *Phys. Rev. Lett.* **84** 4822–5
 Hahn Y 1997 *Rep. Prog. Phys.* **60** 691–759
 Heerlein C, Zwicknagel G and Toepffer 2002 *Phys. Rev. Lett.* **89** 083202

- Hoffknecht A *et al* 1998 *J. Phys. B: At. Mol. Opt. Phys.* **31** 2415–28
- Hoffknecht A *et al* 2000 *Phys. Rev. A* **63** 012702
- Horoj M, Zelevinsky V and Brown B A 1995 *Phys. Rev. Lett.* **74** 5194–7
- Jacquod P and Shepelyansky D L 1997 *Phys. Rev. Lett.* **79** 1837–40
- Karazija R 1991 *Sums of Atomic Quantities and Mean Characteristics of Spectra* (Vilnius: Mokslas)
- Lindroth E, Danared H, Glans P, Pešić Z, Tokman M, Viktor G and Schuch R 2001 *Phys. Rev. Lett.* **86** 5027–30
- Mannervik S, DeWitt D, Engström L, Lidberg J, Lindroth E, Schuch R and Zong W 1998 *Phys. Rev. Lett.* **81** 313–16
- Mirlin A D and Fyodorov Y V 1997 *Phys. Rev. B* **56** 13393–404
- Müller A 1999 *Proc. Trans. R. Soc. A* **357** 1279–96
- Ratcliff K F 1971 *Phys. Rev. C* **3** 117–43
- Rosenzweig N and Porter C E 1960 *Phys. Rev.* **120** 1698–714
- Schippers S, Kieslich S, Müller A, Gwinner G, Schnell M, Wolf A, Covington A, Bannister M E and Zhao L B 2002 *Phys. Rev. A* **65** 042723
- Uwira O *et al* 1997 *Hyperfine Interact.* **108** 149–54
- Zelevinsky V, Brown B A, Frazier M and Horoi M 1996 *Phys. Rep.* **276** 85–176
- Zelevinsky V, Horoi M and Brown B A 1995 *Phys. Lett. B* **350** 141–6